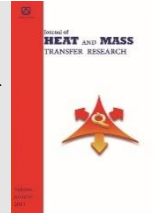




Semnan University



The Effect of Nanoparticle Shape on Hydrothermal Performance and Entropy Generation of Boehmite Alumina Nanofluid in a Cylindrical Heat Sink with Helical Minichannels

Alireza Falahat ^{*a}, Reza Bahoosh ^b

^aDepartment of Mechanical Engineering, Mahshahr Branch, Islamic Azad University, Mahshahr, Iran.

^bDepartment of Mechanical Engineering, Shahid Chamran University of Ahvaz, Ahvaz, Iran.

PAPER INFO

Paper history:

Received: 2021-03-1

Revised: 2022-06-02

Accepted: 2022-06-06

Keywords:

Cylindrical heat sink;
Helical minichannels;
Nanoparticle shape;
Heat transfer;
Entropy generation.

ABSTRACT

In the present paper, heat transfer, fluid flow characteristics, and entropy generation of boehmite alumina nanofluid flowing through a cylindrical helical minichannels heat sink are examined numerically. The evaluated boehmite alumina nanofluid contains dispersed platelets, cylindrical, bricks, and blade nanoparticles in water. This evaluation is performed at two Reynolds number (i.e. $Re=114.5$ and $Re=481.5$) and four nanoparticle volume fraction (i.e., $\varphi = 0, 1\%, 2\%$ and 4%). The numerical results reveal that the heat transfer, friction factor, pumping power, thermal performance factor, and friction entropy generation are augmented and overall thermal resistance, heat transfer entropy generation, total entropy generation, and augmentation entropy generation number are diminished by increasing Reynolds number and nanoparticle volume fraction for all studied shapes of the nanoparticle. The highest and lowest heat transfer, friction factor, pumping power, thermal performance factor, and friction entropy generation relate to the nanofluid containing platelets and bricks shapes nanoparticle, while the maximum and minimum overall thermal resistance, heat transfer entropy generation, and total entropy generation belong to the nanofluid with the bricks and platelets shapes nanoparticle. The highest performance factor was achieved for $\varphi = 4\%$, $Re=114.5$ by using platelets shape nanoparticles and this value is about 1.477.

DOI: [10.22075/jhmtr.2022.22797.1332](https://doi.org/10.22075/jhmtr.2022.22797.1332)

© 2022 Published by Semnan University Press. All rights reserved.

1. Introduction

Thermal-hydraulic performance of micro/minichannel heat sink is taken into consideration for effective cooling of many applications such as microelectronics devices, batteries of electric vehicles, micro reactors and so on, in recent years. Also, another efficient way to enhance the thermal performance of thermal systems is employing nanofluid [1-12].

Peyghambarzadeh et al. [13] examined the thermal-hydraulic performance of Al_2O_3 -water and CuO -water nanofluid in a plain heat sink with 17 microchannels, experimentally. These studies showed that the heat transfer increased with an increase of volume fraction

of nanoparticles in both nanofluid. Also, they indicated that the heat transfer of CuO -water nanofluid was more efficient comparing with Al_2O_3 -water nanofluid. Al-Rashed et al. [14] performed a numerical investigation to evaluate hydrothermal and irreversibility behavior of water-Ag nanofluid inside a heatsink with sinusoidal micorchannels. The results revealed that by increasing the Reynolds number, nanoparticle volume fraction and the wavelength of wavy channel the performance of heatsink enhances. Also, when the amplitude increases and the wavelength decreases, leads to a decrease in the total entropy generation rate. Bahiraei and Heshmatian [15] evaluated the thermal hydraulic and second law characteristics of a new hybrid nanofluid in two new

*Corresponding Author: Alireza Falahat

Email: a_r_falahat@yahoo.com

microchannel heat sinks, numerically. This nanofluid is contained graphene-silver nanoparticles. Their results showed that by increasing inlet velocity and volume fraction of nanoparticles, the maximum surface temperature of both heat sinks decreases. Also, they obtained that the thermal resistance and irreversibility of nanofluid are lower than pure water at constant pumping power.

Alfaryjat et al. [16] numerically examined the effect of several nanofluid (Al_2O_3 , CuO, SiO_2 and ZnO) mixed with water on heat transfer and pressure drop in a microchannel heat sink with a hexagonal cross-section microchannel. They found that Al_2O_3 -water nanofluid has the highest heat transfer coefficient. In addition, they obtained that by decreasing the diameter and increasing the volume fraction of nanoparticles, the thermal resistance of nanofluids is enhanced. Alfaryjat et al. [17] investigated the heat flux and Reynolds number on second law characteristics in a hexagonal microchannel heat sink for various nanofluid (Al_2O_3 , CuO, and SiO_2 -water), numerically. The results revealed that a decrease in heat flux and increase in Reynolds number lead to a decrease in the thermal entropy generation and an increase in heat flux has led to no influence on the frictional entropy generation. Also, they found that SiO_2 -water and Al_2O_3 -water nanofluid had the highest frictional entropy generation and the lowest thermal entropy generation, respectively. Narrein et al. [18] analyzed the heat transfer and pressure drop of Al_2O_3 -water nanofluid in helical minichannel, numerically. They demonstrated that the helical microchannel geometry can enhance the heat transfer and the Nu thermal performance can be further increased by decreasing the helix radius. Al-Rashed et al. [19] investigated the hydrothermal and entropy generation of a biologically synthesized water-silver nanofluid flow in wavy rectangular microchannels numerically. They considered the effect of volume fraction, Reynolds number, and geometrical parameters of the wavy microchannel on the heat transfer coefficient, the surface temperature of the heat sink, pumping power, also thermal, frictional, and total entropy generation. Their results showed that heat transfer was improved with increasing volume fraction and Reynolds number. Also, they found that augmenting the wavelength of the wavy microchannel increases the hydrothermal performance and decreases the total entropy generation. Over the recent decade, several researchers have shown the effect of nanoparticle shapes on enhancing heat transfer.

Elias et al. [20] analytically analyzed the influences of different nanoparticle shapes of boehmite alumina on the performance of a shell and tube heat exchanger. The analytical results revealed that the nanofluid with cylindrical-shaped nanoparticles had a higher heat transfer coefficient and heat transfer rate. Moreover, the entropy generation of nanofluid with cylindrical shaped nanoparticles was higher than other shapes of nanoparticles. Vanaki et al. [21] numerically analyzed the effect of different shapes of nanoparticles on heat transfer and fluid flow of SiO_2 - ethylene glycol nanofluid in a wavy wall channel. They found that the platelet nanoparticle shape has the highest Nusselt

number compared with other nanoparticle shapes. Abassian et al. [22] numerically investigated the effect of boehmite alumina - ethylene glycol and water mixture nanofluid containing six nanoparticle shapes on thermo-hydraulic characteristics in sinusoidal-wavy wall minichannel. They demonstrated that the Nusselt number improves by rising the nanoparticle volume fraction and Reynolds number in all nanoparticle shapes. Liu et al. [23] numerically studied the effect of particle shapes on the thermal performance of Al_2O_3 -water nanofluid in curved square duct by using a two-phase model. The numerical results revealed that with the nanoparticle diameter increment for all particle shapes, the Nusselt number and pressure drop decreased. Also, they found that the nanofluid with the platelet-shaped nanoparticle had the highest heat transfer enhancement, while the nanofluid containing nanoparticles with the brick-shaped nanoparticles demonstrated the lowest pressure drop. Shahsavari et al. [24] numerically evaluated the effects of various nanoparticle shapes on the thermal performance of a boehmite alumina nanofluid in a minichannel double pipe heat exchanger. The authors found that the nanofluid containing platelet-shaped nanoparticles had better heat transfer characteristics, whereas the nanofluid with spherical nanoparticles had a higher performance index. Monfared et al. [25] carried out a numerical study to examine the effects of nanoparticle shape on the second law characteristics of boehmite alumina nanofluid flow in a double pipe heat exchanger. It was revealed that the nanofluid containing platelet shape and spherical shape nanoparticles had the lowest and highest total entropy generation, respectively. Furthermore, they reported that the highest frictional entropy generation rate is achievable with nanofluid containing platelet-shaped nanoparticles. Bahiraei et al. [26] numerically analyzed the effect of the water- Al_2O_3 nanofluid with various nanoparticle shapes on the entropy generation characteristics in a microchannel heat sink. The results demonstrated that the nanofluid having oblate spheroid nanoparticles has the highest entropy generation rather than other nanoparticles. Also, they found that the nanofluid containing the platelet-shaped nanoparticles has the lowest total irreversibility in the greater Reynolds numbers. Zahmatkesh et al. [27] a comprehensive literature review of the effect of nanoparticle shape of nanofluids on the heat transfer and fluid flow of thermal systems. It demonstrated that a promising method for optimization of heat exchange and pumping power is the control of nanoparticle shape.

In recent years, the research on improving heat transfer in the cylindrical heat sink with micro/minichannels for cooling cylindrical heat sources is increasing. Fan et al. [28,29] numerically and experimentally assessed fluid flow and heat transfer characteristics of water flow in a novel cylindrical

minichannel heat sink. The results demonstrated that the heat sink with an oblique fin has a significant heat transfer enhancement with an almost equal pressure drop achieved compared with a conventional heat sink. Azizi et al. [30,31] experimentally examined the thermal and hydraulic characteristics of nanofluid containing Cu nanoparticles in a cylindrical microchannel heat sink. The experimental results indicated that the heat transfer coefficient increases with increasing nanoparticle fraction. Also, they obtained two correlations to predict the Nusselt number and friction factor.

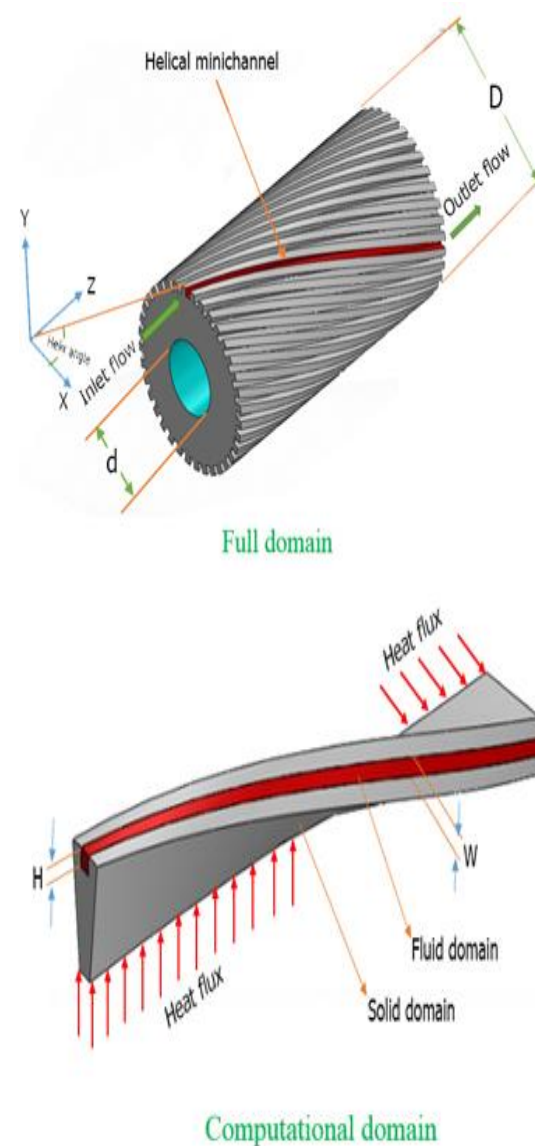
Falahat et al. [32] studied the thermal and hydraulic performance of water flow in a novel cylindrical heat sink with helical minichannels, experimentally. The results showed that decreasing in minichannel helix angle increases the heat transfer and they also developed two new correlations to predict Nusselt number and friction factor in a range of helix angles of 45, 60, and 90 deg. Khalifa and Jaffal [33] numerically and experimentally investigated the effect of channel configuration on the thermal and hydraulic performances of a cylindrical heat sink. The results revealed that the best thermo-hydraulic performance was achieved in the heat sink with a helical minichannel configuration compared with wavy and straight minichannel heat sinks. Abdulhaleem et al. [34] numerically and experimentally studied the hydrothermal and entropy generation of water flow in a cylindrical minichannel heat sink with a hybrid straight-wavy channel. Their results showed that the maximum surface temperature of a hybrid straight-wavy channel decreases significantly in comparison with a straight channel. Moreover, they obtained that the average Nusselt number of the hybrid straight-wavy channel increases by about 20% rather than the straight channel. Bahoosh and Falahat [35] experimentally investigated the Heat transfer, fluid flow characteristics, and entropy generation of water-Al₂O₃ nanofluid flow in cylindrical helical minichannel heat sink with secondary branches. The varied parameters in this investigation were the Reynolds number, helix angle, and volume fraction of nanoparticles. Their experimental results indicated that the secondary branches decreased the Nusselt number and friction factor. The frictional entropy generation rate increases and the thermal entropy generation rate decreases, decreasing the helix angle and increasing the nanoparticles volume fraction. Also, they obtained two new correlations to predict the Nusselt number and friction factor. The literature survey reveals that the effect of nanoparticle shape on the heat transfer and entropy generation in cylindrical helical minichannel heat sink has not been yet assessed. Consequently, in this study, the heat transfer, fluid flow characteristics, and entropy generation of boehmite alumina nanoparticles in cylindrical helical minichannel heat sink are investigated numerically. The effects of various nanoparticle shapes (i.e.

cylindrical, brick, platelet, and blade), nanoparticle volume fraction, and Reynolds number (i.e., $Re=114.5$ and $Re=481.5$) on hydrothermal performance and entropy generation are investigated.

2. Numerical methodology

2.1. Explanation of the geometry

Fig. 1. demonstrates the schematic diagram of the cylindrical helical minichannel heat sink, which includes 36 helical minichannels and computational domain followed in this study. The boehmite alumina and the copper are chosen as the cooling fluid and the heat sink material, respectively. To reduce simulation time, one helical minichannel is simulated periodically in three dimensional as the computational domain. The computational domain comprises of fluid and solid part. The geometric parameters of the cylindrical helical minichannel heat sink are shown in Table 1.



(a)

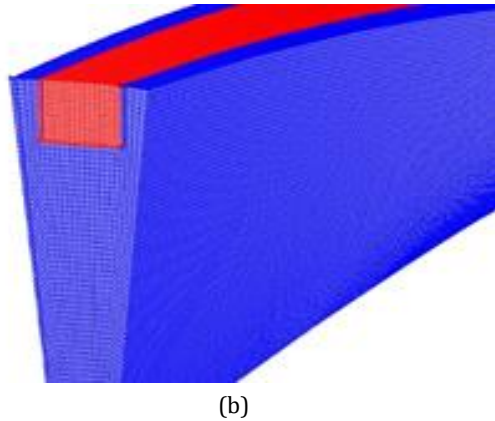


Figure 1. (a) Schematic diagram of studied cylindrical helical minichannel heat sink and (b) schematic view of the three-dimensional mesh

Table 1. Geometric parameters of cylindrical helical minichannel heat sink.

Geometric parameter	Value
S (mm)	50
D (mm)	25
d (mm)	10
H (mm)	1.2
W (mm)	1
Helix angle (degree)	50
N	36

2.2. Governing equations and boundary conditions

For the simplicity of analyzing the thermal-hydraulic characteristics of the cylindrical heat sink, the following assumptions were considered: The nanofluid is assumed to be single-phase, Newtonian, incompressible and steady-state nature. The effect of natural convection and radiation are ignored. The effects of viscous dissipation are negligible [36]. The thermophysical properties of the fluid and solid domain are temperature dependent and constant, respectively. Under the aforementioned assumptions, the following equations must be resolved for fluid and solid:

Continuity equation:

$$\frac{\partial u}{\partial x} + \frac{\partial v}{\partial y} + \frac{\partial w}{\partial z} = 0 \quad (1)$$

Momentum equation:

$$\rho_{nf} \left(u \frac{\partial u}{\partial x} + v \frac{\partial u}{\partial y} + w \frac{\partial u}{\partial z} \right) = -\frac{\partial P}{\partial x} + \mu_{nf} \left(\frac{\partial^2 u}{\partial x^2} + \frac{\partial^2 u}{\partial y^2} + \frac{\partial^2 u}{\partial z^2} \right) \quad (2a)$$

$$\rho_{nf} \left(u \frac{\partial v}{\partial x} + v \frac{\partial v}{\partial y} + w \frac{\partial v}{\partial z} \right) = -\frac{\partial P}{\partial y} + \mu_{nf} \left(\frac{\partial^2 v}{\partial x^2} + \frac{\partial^2 v}{\partial y^2} + \frac{\partial^2 v}{\partial z^2} \right) \quad (2b)$$

$$\rho_{nf} \left(u \frac{\partial w}{\partial x} + v \frac{\partial w}{\partial y} + w \frac{\partial w}{\partial z} \right) = -\frac{\partial P}{\partial z} + \mu_{nf} \left(\frac{\partial^2 w}{\partial x^2} + \frac{\partial^2 w}{\partial y^2} + \frac{\partial^2 w}{\partial z^2} \right) \quad (2c)$$

Energy equation for fluid:

$$\rho_{nf} c_{p,nf} \left(u \frac{\partial T}{\partial x} + v \frac{\partial T}{\partial y} + w \frac{\partial T}{\partial z} \right) = k_{nf} \left(\frac{\partial^2 T}{\partial x^2} + \frac{\partial^2 T}{\partial y^2} + \frac{\partial^2 T}{\partial z^2} \right) \quad (3)$$

Energy equation for solid:

$$k_s \left(\frac{\partial^2 T}{\partial x^2} + \frac{\partial^2 T}{\partial y^2} + \frac{\partial^2 T}{\partial z^2} \right) = 0 \quad (4)$$

where, ρ , k , c_p , μ , P , u , v , w and T demonstrate the density, thermal conductivity, constant pressure specific heat, dynamic viscosity, pressure, x component, y component and z component of velocity and temperature, respectively. Also, subscripts nf and s indicate the nanofluid and solid, respectively. The hydrodynamic and thermal boundary conditions for simulations are listed in Table 2.

Table 2. Applied boundary conditions for simulations.

Location	Boundaries conditions
Inlet of minichannel	Uniform velocity and uniform temperature ($T_{in} = 297 \text{ K}$)
Outlet of minichannel	Pressure outlet ($P_{out} = 0$)
Heated wall of heat sink	$q'' = -k_s \nabla T_s = 190 \text{ W/cm}^2$
fluid–solid interface	$-k_s \nabla T_s = -k_f \nabla T_f$ and $T_f = T_s$
Side walls of substrate heat sink	Periodic
All other walls	Adiabatic

2.3. Numerical data processing

2.3.1. Heat transfer and fluid flow

For measurement of nanofluid temperature, mass-weighted average value was used, while area-weighted average value was used for temperature of minichannel wall, pressure and velocity of nanofluid.

The hydraulic diameter and Reynolds number of minichannel can be defined as:

$$D_h = \frac{2WH}{(W + H)} \quad (5)$$

$$Re = \frac{\rho_{nf} v_m D_h}{\mu_{nf}} \quad (6)$$

where, v_m represents the fluid average velocity over the minichannel cross-sectional area.

The Fanning friction factor and pumping power [15] are defined by:

$$f = \frac{\Delta P D_h}{2L\rho_{nf}v_m^2} \quad (7)$$

$$PP = NA_c v_m \Delta P \quad (8)$$

where, $\Delta P = P_{in} - P_{out}$, N and L are the pressure drop along the helical minichannel, number of minichannels and length of minichannel, respectively.

The average Nusselt number and heat transfer coefficient are written as:

$$Nu = \frac{hD_h}{k_{nf}} \quad (9)$$

$$h = \frac{q}{A_{ht}[T_w - T_f]} \quad (10)$$

where, $q, T_w, T_f = 0.5 (T_{in} + T_{out})$ and A_{ht} are the heat transfer absorbed by nanofluid, the average wall temperature, average fluid flow temperature and the heat transfer area of helical minichannel, respectively.

The overall thermal resistance can be obtained by [37,38]:

$$R_{th} = \frac{T_{w,max} - T_{in}}{q} \quad (11)$$

where, $T_{w,max}$ is the maximum wall temperature of helical minichannel.

The thermal performance factor [39] is given by:

$$JF = (Nu_{nf}/Nu_f) \times (f_{nf}/f_f)^{-1/3} \quad (12)$$

where, subscript f represents the water as base fluid.

2.3.2. Entropy generation

The other way to estimate performance of minichannels heat sink is study of entropy generation. The irreversibility related with the flow and heat transfer processes in micro/minichannel heat sink devices can be determined by computing the total volume entropy generation rates [40]:

$$\dot{S}_{gen} = \dot{S}_{gen,T} + \dot{S}_{gen,P} \quad (13)$$

$$\dot{S}_{gen,T} = \frac{k_{nf}}{T^2} \left[\left(\frac{\partial T}{\partial x} \right)^2 + \left(\frac{\partial T}{\partial y} \right)^2 + \left(\frac{\partial T}{\partial z} \right)^2 \right] \quad (14)$$

$$\dot{S}_{gen,P} = \frac{\mu_{nf}}{T} \left\{ 2 \left[\left(\frac{\partial u}{\partial x} \right)^2 + \left(\frac{\partial v}{\partial y} \right)^2 + \left(\frac{\partial w}{\partial z} \right)^2 \right] + \left(\frac{\partial u}{\partial y} + \frac{\partial v}{\partial x} \right)^2 + \left(\frac{\partial u}{\partial z} + \frac{\partial w}{\partial x} \right)^2 + \left(\frac{\partial v}{\partial z} + \frac{\partial w}{\partial y} \right)^2 \right\} \quad (15)$$

where, $\dot{S}_{gen}, \dot{S}_{gen,T}$ and $\dot{S}_{gen,P}$ are the rate of local total entropy generation, rate of local heat transfer entropy generation and rate of local fluid friction entropy generation, respectively.

By integration Eqs. (13), (14) and (15) over whole domain, determined the rate of total entropy generation, heat transfer entropy generation and fluid flow entropy generation, respectively. The detailed derivation method of equation (16) was reported in Ref [41]:

$$S_{gen} = \frac{q(T_w - T_f)}{T_w T_f} + \frac{Q}{T_f} \Delta P \quad (16)$$

where, Q is volumetric flow rate. The augmentation entropy generation number can be calculated to compare the total entropy generation rate of nanofluid ($S_{gen,nf}$) to the base fluid ($S_{gen,f}$), which is defined by [42]:

$$N_s = \frac{S_{gen,nf}}{S_{gen,f}} \quad (17)$$

2.4. Thermophysical properties of nanofluid

In the present research, the water based nanofluid with boehmite alumina nanoparticles are investigated. The temperature-dependent thermophysical properties of water are reported in Table 3. And the thermophysical properties of nanoparticle are represented in Table 4.

In order to quantitatively evaluate for instance in the nanofluid volume concentration of 4.0%, the required mass of (γ -AlOOH) nanoparticles for preparing 1 liter of nanofluid, according to the equation mentioned in the ref [45] is equal to 122 grams.

The density and specific heat of nanofluid are defined as follows [46]:

$$\rho_{nf} = (1 - \varphi)\rho_f + \varphi\rho_{np} \quad (18)$$

$$\rho_{nf}C_{p,nf} = (1 - \varphi)\rho_fC_{p,f} + \varphi\rho_{np}C_{p,np} \quad (19)$$

where, φ is the volume fraction. Also, subscript np represents to nanoparticle.

In the present work, four shapes of nanoparticles (i.e. Cylindrical, Brick, Blade and Platelet) are investigated. The thermal conductivity and viscosity of nanofluid for non-spherical shapes of nanoparticles are calculated by following equations [21,22]:

$$k_{nf} = k_f(1 + C_k\varphi) \quad (20)$$

$$\mu_{nf} = \mu_f(1 + A_1\varphi + A_2\varphi^2) \quad (21)$$

where, C_k, A_1 and A_2 are constant coefficient which are available in Table 5.

Table 3. Temperature-dependent thermophysical properties of water [43]

T(K)	ρ (kg/m ³)	C_p (J/kgK)	k (W/mK)	μ (kg/ms)
293	998.2	4183	0.599	0.001004
303	995.7	4174	0.618	0.000802
313	992.2	4174	0.635	0.000653
323	988.1	4174	0.648	0.000549
333	983.1	4179	0.659	0.000469

Table 4. Thermophysical properties of boehmite alumina nanoparticles [44]

ρ (kg/m ³)	3050
C_p (J/kgK)	618.3
k (W/mK)	30

Table 5. Thermal conductivity and viscosity coefficient for various nanoparticle shapes [47]

Type	ψ	C_k	A_1	A_2
Platelets	0.52	2.61	37.1	612.6
Blades	0.36	2.74	14.6	123.3
Cylindrical	0.62	3.95	13.5	904.4
Bricks	0.81	3.37	1.9	471.4

2.5. Solution procedure and validation

The governing equations (Eqs. (1)-(4)) were discretized using the commercial software Fluent 15 in computational domain and solve these equations along with appropriate boundary conditions. The SIMPLE algorithm and standard scheme were used for coupling of velocity and discretization of pressure, respectively. The second-order upwind method were applied to discretize the convective term of momentum and energy equations. The governing equations are solved by a segregated implicit iterative scheme. The convergence criteria for the continuity, momentum and energy equations are considered smaller than 1×10^{-6} , 1×10^{-6} , and 1×10^{-9} , respectively.

For reduce computational cost and to ensure the accurate solution, the grid independence test was carried out for entire computational domain. Four sets of grid numbers i.e., 555104, 1095600, 1743000 and 2340000 with structured hexahedral mesh were generated (see Fig. 1 (b)). And their corresponding Nusselt number and pressure drop were compared at $Re = 398.9$. The relative errors in the Nusselt number and pressure drop were calculated (Table 6). It was found that increasing grid sizes from 1743000 grids did not lead to significant difference in the Nusselt number and pressure drop as it is shown in Table 6. So, the grid system 3 (1743000 grids) was adopted for computation.

For validation the reliability and accuracy of the numerical method, the average Nusselt number and Fanning friction factor have been compared with correlations of Falahat et al. [32]. Fig. 2(a) and (b) represent good agreement between the numerical results with Falahat et al. [32]. The average deviation of Nusselt number and Fanning friction factor are about 4.5% and 7.4%, respectively.

Table 6. Grid independence results.

Grid system	Number of grid	Nu	$E_{Nu}\%$	$\Delta P(Pa)$	$E_{\Delta P}\%$
Grid 1	555104	9.41	2.84	385.75	6.51
Grid 2	1095600	9.34	2.08	408.25	1.06
Grid 3	1743000	9.19	0.44	411.85	0.19
Grid 4	2324000	9.15	baseline	412.62	baseline

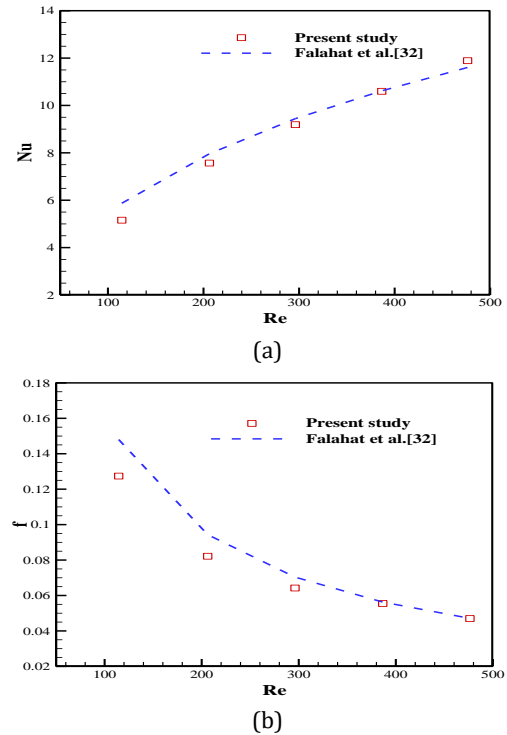


Figure 2. Comparison of numerical results with correlations of Falahat et al. [32]; (a) Nusselt number, (b) Fanning friction factor

3. Results and discussion

In the present work, the hydrothermal performance and entropy generation of boehmite alumina nanoparticles are carried out in cylindrical helical minichannel heat sink. The nanoparticle shapes of cylindrical, brick, platelet and blade are considered. The numerical investigations are performed at nanoparticle volume fraction of 0, 1%, 2% and 4%, Reynolds number 114.5 and 481.5.

Figures 3(a) and 3(b) illustrate the Nusselt number of boehmite alumina nanofluid containing various shapes of nanoparticles versus nanoparticle volume fraction for Reynolds numbers of 114.5 and 481.5, respectively. It can be seen that the Nusselt number increases with an increase volume fraction of nanoparticle in fixed Reynolds number for all shape of nanoparticles. The reason is the increment of the nanofluid thermal conductivity with increasing of nanoparticle volume fraction and also, with increasing volume fraction of nanoparticle in all shapes of nanoparticle leads to the increment nanofluid velocity in fixed Reynolds number, as a result, the thermal boundary layer diminishes and the heat transfer is enhanced. It is clear that the nanofluids with platelets, cylindrical, blades and bricks shaped nanoparticles have the highest to lowest Nusselt number in both Reynolds number and at nanoparticles volume fractions of 1% to 4%. The Similar result were reported by Vanaki et al. [21]. For nanofluid containing blades and bricks nanoparticle, the Nusselt number increases

as volume fraction of nanoparticle grows from 1% to 4%, but the growth rate is smaller than platelets and cylindrical shaped nanoparticles in Reynolds number 114.5 and 481.5. It should be noted that, at volume fraction of 4%, the Nusselt number of blades and bricks shaped nanoparticles is approximately equal. The results indicated that with increasing Reynolds number from 114.5 to 481.5 in fixed volume fraction of nanoparticle and studied shaped nanoparticles, the Nusselt number increases, because the increment of nanofluid velocity and consequently, the velocity boundary layer is decreases and leads to reduction thermal boundary layer of nanofluid. For better discussion of result, the average velocity of nanofluids at Reynolds 481.5 and nanoparticle volume fraction of 4% is indicated in Table 7 for all studied nanoparticles shapes. It can be observed from this Table, the velocity of nanofluid containing platelets shaped nanoparticles is highest among other nanofluids. As an illustration, at the Reynolds number of 114.5 and nanofluid containing platelets shaped nanoparticle (Fig. 3 (a)), the Nusselt number in nanoparticle volume fraction of 1%, 2% and 4% is 17.65%, 31.64% and 55.61% higher than the base fluid, respectively. Also, at Reynolds number of 481.5 and nanoparticle volume fraction of 4%, the Nusselt number of nanofluid containing platelets (Fig. 3 (b)), cylindrical, blade and bricks nanoparticles shape is 34.14%, 27.44%, 11.81% and 11.99% higher than the base fluid, respectively.

Table 7. The average velocity of nanofluid containing various nanoparticle shapes at $Re=481.5$ and $\phi = 4\%$.

Nanoparticle shape	Velocity (m/s)
Platelet	1.288
Cylindrical	1.109
Brick	0.672
Blade	0.653

Figures 4(a) and 4(b) show the variation of the friction factor of boehmite alumina nanofluid in different shapes of nanoparticles versus nanoparticle volume fraction for Reynolds numbers of 114.5 and 481.5, respectively. It is observed that the friction factor increases with increasing nanoparticle volume fraction and it has a similar trend for studied nanoparticle shapes. In the same Reynolds number, the nanofluid containing bricks, blades, cylindrical and platelets nanoparticles shape have the lowest to highest friction factor. In view of the fact, at constant nanoparticle volume fraction and Reynolds number, the platelets nanoparticle shape has the highest viscosity followed by the cylindrical, blades and bricks nanoparticle shape, respectively. On this basis, the velocity of nanofluid with platelets, cylindrical, blades and bricks nanoparticles shape is the highest to lowest value, respectively and consequently the pressure losses and friction factor are increased. At both Reynolds numbers of 114.5 and 481.5, the friction factor of nanofluid with platelets particle shape and

nanoparticle volume fraction of 4% is 4.11% and 1.30% greater than the base fluid, respectively. Also, at Reynolds of 114.5 and nanoparticle volume fraction of 4%, the friction factor of nanofluid with platelets, cylindrical, blades and bricks increases 4.11%, 3.83%, 3.06% and 3.29% rather than the base fluid, respectively.

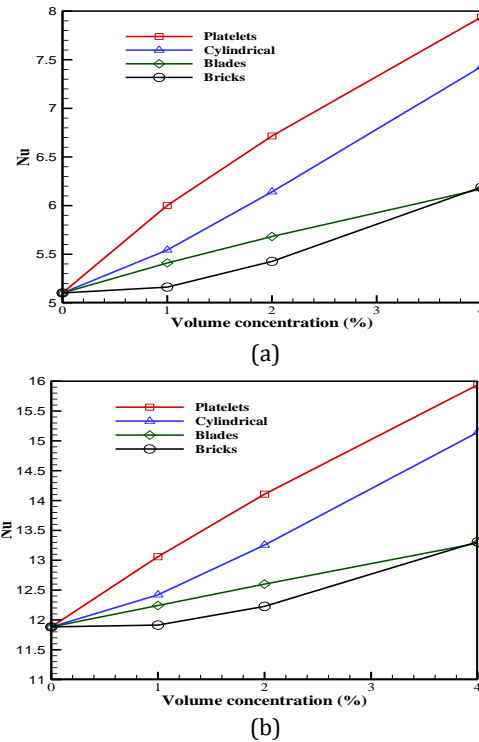


Figure 3. The effect of various nanoparticle shapes on Nusselt number at (a) $Re=114.5$ and (b) $Re=481.5$

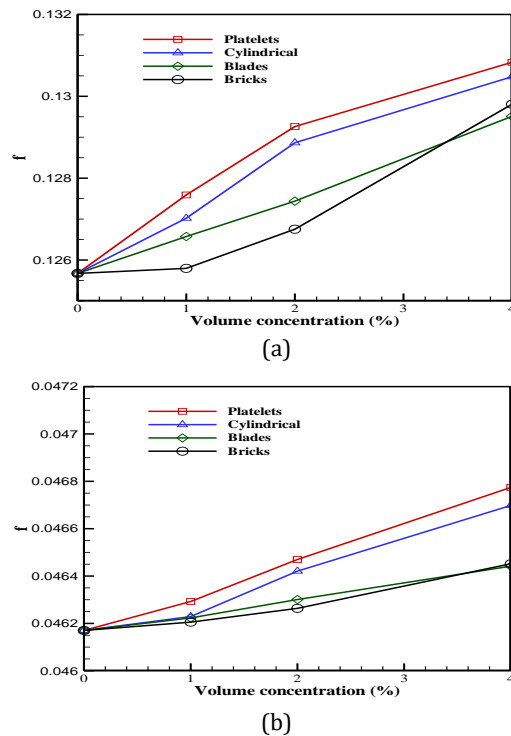


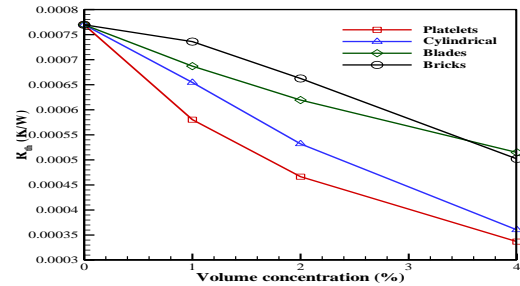
Figure 4. The effect of various nanoparticle shapes on friction factor at (a) $Re=114.5$ and (b) $Re=481.5$

Figures 5(a) and 5(b) demonstrate the variation of the overall thermal resistance of boehmite alumina nanofluid in different shapes of nanoparticles versus nanoparticle volume fraction for Reynolds numbers of 114.5 and 481.5, respectively. The overall thermal resistance decreases with increasing nanoparticle volume fraction and increasing Reynolds number for all nanoparticles shapes and exhibits a similar trend at all studied shapes. The overall resistance of nanofluid with platelets shape nanoparticle is lower than other nanoparticles shapes. It should be noted that a small overall thermal resistance is indicated uniform temperature distribution and is improved heat transfer in heat sink. For example, the lowest overall resistance is observed for Reynolds number 114.5 and nanoparticle volume fraction of 4%, as the reduction is 55.84% in platelets shape, 52.25% in cylindrical shape, 33.12% in blades shape and 34.81% in bricks shape compared to the base fluid.

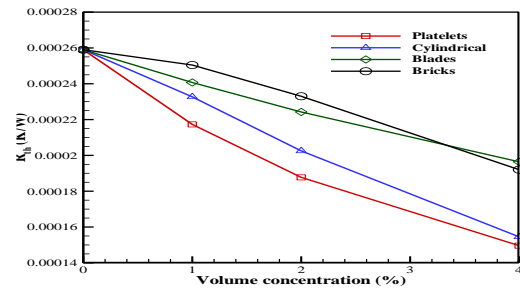
Figures 6(a) and 6(b) indicate the pumping power against the volume fraction of nanoparticles and Reynolds numbers 114.5 and 481.5 for all the studied nanoparticles shapes. According to the results, the pumping power increases with the increase in nanoparticle volume fraction and Reynolds number. Among various nanofluid, the nanofluid with platelets and bricks shape nanoparticles has the highest and the lowest pumping power in all nanoparticle volume fraction and both Reynolds number. It is seen that, for nanofluid with platelets shape nanoparticles at nanoparticle volume fraction of 4% , the pumping power is 6027.6% and 3888.3 higher than base fluid for Reynolds number 114.5 and 481.5, respectively. Also, the pumping power augments 3037.6% by rising Reynolds number from 114.5 to 481.5 for nanofluid with platelets shape nanoparticles and nanoparticle volume fraction of 4%. In view of the fact, the nanofluid with platelets shape nanoparticles has highest pressure drop and volume flow rate than other studied nanofluids and base fluid.

Figures 7(a) and 7(b) indicate the thermal performance factor against the volume fraction of nanoparticles and the Reynolds numbers 114.5 and 481.5 for different shapes of nanoparticles. According to these figures, the thermal performance factor increases with volume fraction of nanoparticles in different shapes of nanoparticles and both Reynolds number. This phenomenon is due to the fact that the adding nanoparticles enhances the heat transfer more than pressure drop increasing. Also, it can be seen that the thermal performance factor decreases with increasing Reynolds number in all shapes of nanoparticles and fixed volume fraction of nanoparticles, which are main causes for this behavior, is increasing pressure drop significantly with increment of Reynolds number. For example, the thermal performance factor of nanofluid with cylindrical shape nanoparticle and nanoparticles

volume fraction of 4% is 1.39 and 1.26 for Reynolds number of 114.5 and 481.5, respectively. The results indicate that the nanofluid with platelets and bricks shape nanoparticles has highest and lowest thermal performance factor in all volume fraction of nanoparticles and the Reynolds numbers 114.5 and 481.5, respectively. For instance, in nanoparticles volume fraction of 4% and Reynolds number of 114.5, the thermal performance factor of nanofluid with platelets and bricks shape nanoparticles is 1.48 and 1.16, respectively.

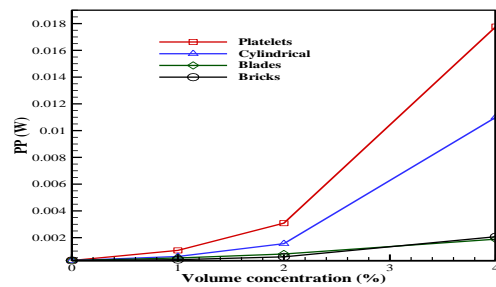


(a)

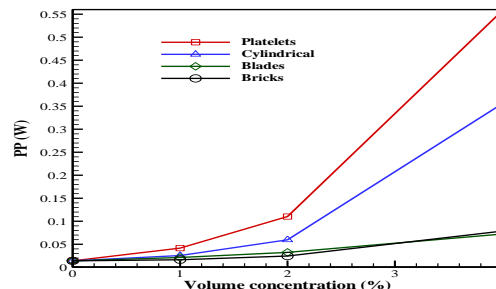


(b)

Figure 5. The effect of various nanoparticle shapes on overall thermal resistance at (a) Re=114.5 and (b) Re=481.5



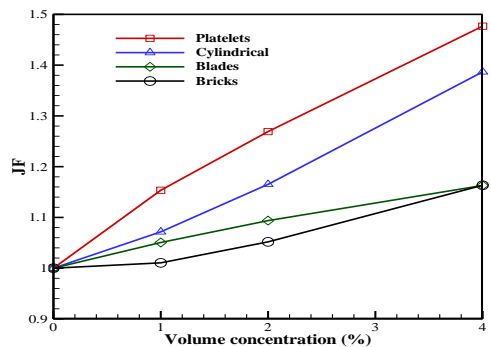
(a)



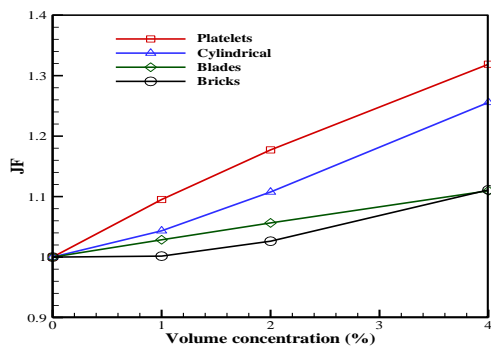
(b)

Figure 6. The effect of various nanoparticle shapes on pumping power at (a) Re=114.5 and (b) Re=481.5

Figures 7(a) and 7(b) indicate the thermal performance factor against the volume fraction of nanoparticles and the Reynolds numbers 114.5 and 481.5 for different shapes of nanoparticles. According to these figures, the thermal performance factor increases with volume fraction of nanoparticles in different shapes of nanoparticles and both Reynolds number. This phenomenon is due to the fact that the adding nanoparticles enhances the heat transfer more than pressure drop increasing. Also, it can be seen that the thermal performance factor decreases with increasing Reynolds number in all shapes of nanoparticles and fixed volume fraction of nanoparticles, which are main causes for this behavior, is increasing pressure drop significantly with increment of Reynolds number. For example, the thermal performance factor of nanofluid with cylindrical shape nanoparticle and nanoparticles volume fraction of 4% is 1.39 and 1.26 for Reynolds number of 114.5 and 481.5, respectively. The results indicate that the nanofluid with platelets and bricks shape nanoparticles has highest and lowest thermal performance factor in all volume fraction of nanoparticles and the Reynolds numbers 114.5 and 481.5, respectively. For instance, in nanoparticles volume fraction of 4% and Reynolds number of 114.5, the thermal performance factor of nanofluid with platelets and bricks shape nanoparticles is 1.48 and 1.16, respectively.



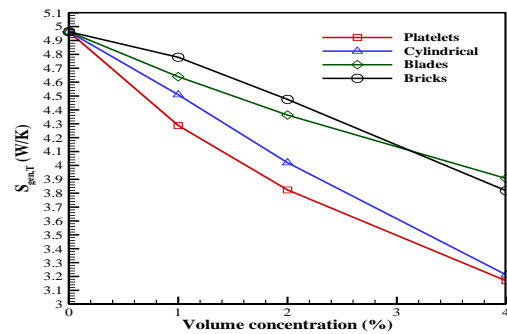
(a)



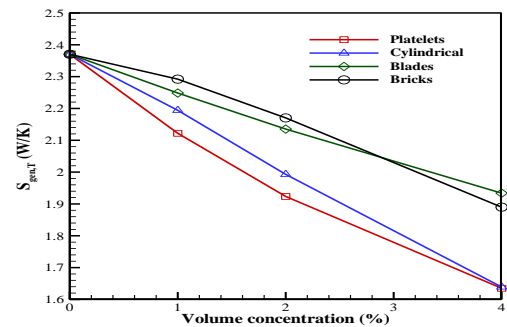
(b)

Figure 7. The effect of various nanoparticle shapes on thermal performance factor at (a) Re=114.5 and (b) Re=481.5

Figures 8(a) and 8(b) demonstrate the variation of the heat transfer entropy generation of boehmite alumina nanofluid in different shapes of nanoparticles against nanoparticle volume fraction for Reynolds numbers of 114.5 and 481.5, respectively. As observed, the heat transfer entropy generation decreases with increment of nanoparticle volume fraction and Reynolds number for all studied nanoparticle shapes, it is worth mentioning, the value of the reduction is significant. Also, it can be observed that in all nanoparticle volume fraction and both Reynolds number, the nanofluids with platelets and bricks shapes nanoparticles have lowest and lowest highest heat transfer entropy generation. At nanoparticle volume fraction 1 to 4% and Reynolds number 114.5, the heat transfer entropy generation for nanofluids containing platelets shape nanoparticles is 13.61% - 36.15% smaller than the base fluid, whereas this reduction at Reynolds number 481.5 is 10.48% and 31.02%, respectively. The reason is that by increasing the nanoparticle volume fraction at a constant Reynolds number leads to the enhancement in temperature gradient and, consequently, the thickness of thermal boundary layer is decreased and accordingly, the heat transfer entropy generation decreases by increment of nanoparticle volume fraction. Also, the reduction of the heat transfer entropy generation in fixed Reynolds number of 481.5 and nanoparticle volume fraction of 4% for nanofluids with platelets, cylindrical, blades and bricks shape nanoparticles is 31.02%, 31.2%, 18.41% and 20.3% rather than the base fluid, respectively.



(a)



(b)

Figure 8. The effect of various nanoparticle shapes on heat transfer entropy generation at (a) Re=114.5 and (b) Re=481.5

Figures 9(a) and 9(b) show the variation of the friction entropy generation of boehmite alumina nanofluid for all nanoparticles shapes against nanoparticle volume fraction for Reynolds numbers of 114.5 and 481.5, respectively. It can be seen that the friction entropy generation heightens with increasing nanoparticle volume fraction for all shapes of nanoparticles, so that its changes are high by the variations of nanoparticle volume fraction, especially for nanofluids with platelets and cylindrical shape nanoparticles in both Reynolds number. By rising the nanoparticle volume fraction from 1 to 4% at Reynolds number 114.5, the friction entropy generation of nanofluids with platelets, cylindrical, blades and bricks shape nanoparticles is increased by 1619.9%, 1786.8%, 295.4% and 493.4%, respectively, whereas this reduction at Reynolds number 481.5 is 1243.6%, 1296.5%, 239.7% and 382%, respectively. In fact, with increasing the nanoparticle volume fraction in fixed Reynolds number, the nanofluid velocity increases, consequently, the pressure drop increases (related to Eq. (16)); and leads to the increase in the friction entropy generation. This finding Correspond to the results reported by Monfared et al. [19]. Furthermore, the results indicate that with increasing Reynolds number in fixed nanoparticle volume fraction for all shapes of nanoparticles, the friction entropy generation increases. For instance, at fixed nanoparticle volume fraction of 2%, with increasing Reynolds number from 114.5 to 481.5, the friction entropy generation of nanofluids containing platelets, cylindrical, blades and bricks shape nanoparticles is increased 3523%, 3810.3%, 4151% and 4328.8%, respectively. The reason is that the nanofluid velocity increases with increasing the Reynolds number, the velocity gradient is augmented and leads to increasing the friction entropy generation.

Figures 10(a) and 10(b) display the total entropy generation of boehmite alumina nanofluid against nanoparticle volume fraction in different nanoparticles shapes for Reynolds numbers of 114.5 and 481.5, respectively. It is clear that the total entropy generation decreases by elevation of nanoparticle volume fraction and Reynolds number. Obviously, the trend of variation in the total entropy generation obeys the heat transfer entropy generation. Also, it is observed that the lowest and highest total entropy generation related to nanofluids containing platelets and bricks shape nanoparticles in all nanoparticle volume fraction an both Reynolds number, respectively. According to these figures, based on the entropy generation, the nanofluid with platelets shape of boehmit alumina nanoparticles in the greater Reynolds number is the optimal choice because results in minimum total entropy generation in all nanoparticle volume fraction, compared to the other studied shape nanoparticles.

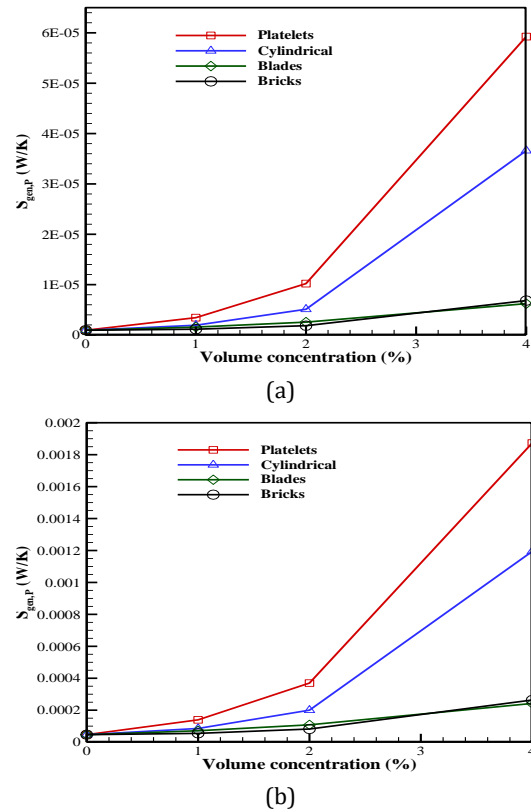


Figure 9. The effect of various nanoparticle shapes on friction entropy generation at (a) Re=114.5 and (b) Re=481.5

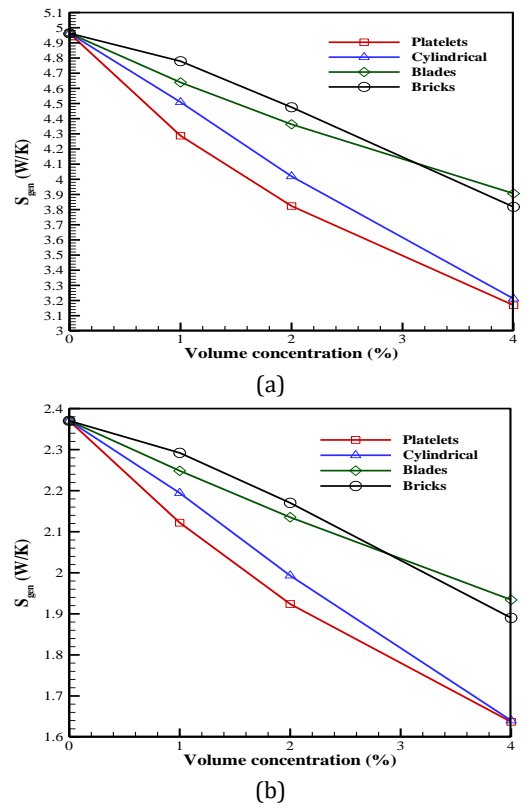


Figure 10. The effect of various nanoparticle shapes on total entropy generation at (a) Re=114.5 and (b) Re=481.5

Figures 11(a) and 11(b) exhibit the variation of the augmentation entropy generation number against nanoparticle volume fraction in different nanoparticles shapes for Reynolds numbers of 114.5 and 481.5, respectively. The best performance of helical minichannels heat sink is achieved in the augmentation entropy generation number of lower than unity. This means that the total entropy generation of nanofluids in helical minichannels is lower than the total entropy generation of the base fluid in all studied nanoparticle volume fraction and both Reynolds number. At a constant Reynolds number, by rising the volume fraction of nanoparticles, the viscosity of the nanofluid increases, which increases the average velocity of the nanofluid. Thereby, the temperature gradients reduce which decreases the heat transfer entropy generation (see equation (14)) and the velocity gradients increase which increases the fluid friction entropy generation (see equation (15)). The contribution of the heat transfer entropy generation is more significant than that the fluid friction entropy generation. So, the total entropy generation of nanofluid with different shapes of nanoparticles rather than base fluid decreases and the augmentation entropy generation number decreases.

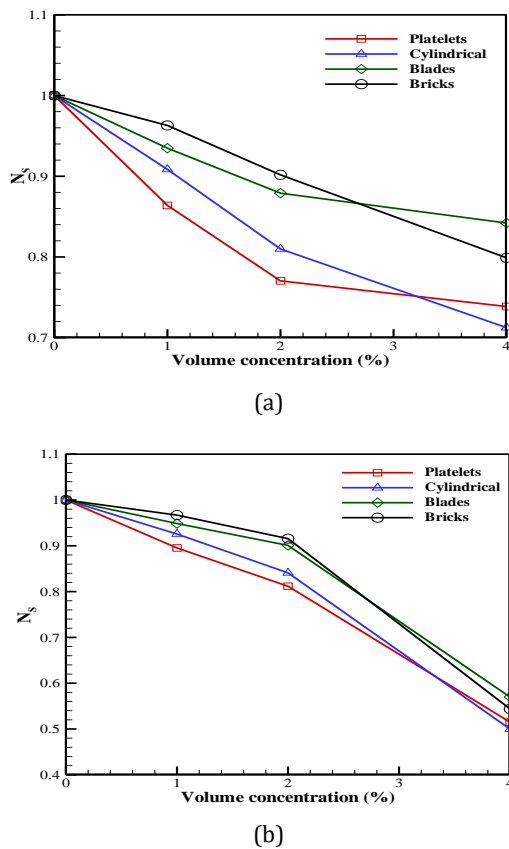


Figure 11. The effect of various nanoparticle shapes on augmentation entropy generation number at (a) $Re=114.5$ and (b) $Re=481.5$

The velocity value for nanofluids with different nanoparticle shapes in a constant volume fraction of nanoparticles depends on the value of viscosity, this. According to Table 7, the nanofluid containing the Platelet shape nanoparticles has the highest average velocity, thus having the lowest the total entropy generation and the augmentation entropy generation number. At a constant the volume fraction of nanoparticles and the all of nanoparticles shapes, the increment of the Reynolds number leads to the total entropy generation of nanofluids and the augmentation entropy generation number decrease. The results indicate that the augmentation entropy generation number decreases with increasing nanoparticle volume fraction and Reynolds number for all studied shape of nanoparticle. Also, it can be concluded that the nanofluids with platelets shape nanoparticles have a lower the augmentation entropy generation number than other kinds of nanofluids.

Conclusions

In this present research, the effects of different nanoparticle shapes of boehmit alumina nanofluids on the heat transfer, fluid flow characteristics and entropy generation in cylindrical heat sink with helical minichannels were numerically studied. The remarkable conclusions of this numerical research are as follows:

- The heat transfer is increased by the increment of Reynolds number for all shapes of nanoparticle.
- The friction factor is increased by the nanoparticle volume fraction and Reynolds number for all studied shapes nanoparticle.
- The maximum heat transfer and friction factor related to the nanofluid with the platelets shapes nanoparticle followed by the cylindrical, blades and bricks shapes nanoparticle, respectively.
- The nanofluids with the platelets and bricks shapes nanoparticle have a highest and lowest the pumping power in all nanoparticle volume fraction and Reynolds number, respectively.
- The overall thermal resistance is decreased with increasing nanoparticle volume fraction and Reynolds number for all nanoparticles shapes and the nanofluid with the platelets shapes nanoparticle has a lowest overall resistance in all nanoparticle volume fraction and Reynolds number.
- The thermal performance factor of nanofluids is increased with increasing nanoparticle volume fraction in all shapes of nanoparticle.
- The thermal performance factor of nanofluids is decreased with increasing Reynolds number in all nanoparticle volume fraction and all shapes of nanoparticle.

- With increment in nanoparticle volume fraction and Reynolds number, the heat transfer entropy generation is decreases and the friction entropy generation is increased for all shapes of nanoparticle.
- The total entropy generation is decreased with the increment of nanoparticle volume fraction and Reynolds number for all shapes of nanoparticle and the nanofluids with the platelets and bricks shapes nanoparticles have a lowest and highest the total entropy generation.
- From the viewpoint of entropy generation, the best and worst performance is related to the nanofluids with the platelets and bricks shape nanoparticles.

Nomenclature

A_C	Cross section area of minichannel, m^2
A_{ht}	Heat transfer area of minichannel, m^2
C_p	Specific heat transfer, $J/kg\ K$
D_h	Hydraulic diameter, m
f	Fanning friction factor
H	Minichannel Height, m
h	Heat transfer coefficient, $W/m^2\ K$
JF	Thermal performance factor
k	Thermal conductivity, $W/m\ K$
L	Minichannel length, m
N	Number of minichannel
N_s	augmentation entropy generation number
Nu	Nusselt number
P	Pressure, Pa
PP	Pumping power, W
Pr	Prandtl number
q	heat transfer absorbed by nanofluid, W
Q	Volumetric flow rate, m^3/s
R_{th}	Overall thermal resistance, K/W
Re	Reynolds number
S	Heat sink length, m
\dot{S}_{gen}	Local total entropy generation rate, $W/m^3\ K$
S_{gen}	Total entropy generation rate, W/K
T	Temperature, K
V	Velocity, m/s
v_m	Average velocity, m/s
W	Minichannel width, m

Greek symbols

μ	Dynamic viscosity, $Pa.s$
ρ	Density, kg/m^3
φ	Volume concentration

Subscripts

f	Fluid
-----	-------

in	Inlet
max	Maximum
nf	Nanofluid
np	Nanoparticle
out	Outlet
s	Solid
w	Wall

References

- [1] Zeinali Heris, S., Noie, S.H., Talaii, E. and Sargolzaei, J., 2011. Numerical investigation of Al₂O₃/water nanofluid laminar convective heat transfer through triangular ducts. *Nanoscale Research Letters*, 179(6), pp.1-10.
- [2] Zeinali Heris, S., Kazemi-Beydokhti, A., Noie, S. H. and Rezvan, S., 2012. Numerical study on convective heat transfer of Al₂O₃/water, CuO/water and Cu/water nanofluids through square cross-section duct in laminar flow. *Engineering Applications of Computational Fluid Mechanics*, 6(1), pp.1-14.
- [3] Tajik Jamal-Abad, M., Dehghan, M., Saedodin, S., Valipour, M.S. and Zamzamin, A.M., 2014. An experimental investigation of rheological characteristics of non-Newtonian nanofluids. *Journal of Heat and mass transfer research*, 1(1), pp. 17-23.
- [4] M. Kahani, M., Zeinali Heris, S. and Mousavi, S.M., 2013. Comparative study between metal oxide nanopowders on thermal characteristics of nanofluid flow through helical coils. *Powder Technology*, 246, pp. 82-92.
- [5] Zeinali Heris, S., Nassan, T.H., Noie, S.H., Sardarabadi, H. and Sardarabadi, M., 2013. Laminar convective heat transfer of Al₂O₃/water nanofluid through square cross-sectional duct. *International Journal of Heat and Fluid Flow* 44, pp. 375-382.
- [6] Kahani, M., Zeinali Heris, S. and Mousavi, S.M., 2013. Effects of curvature ratio and coil pitch spacing on heat transfer performance of Al₂O₃/water nanofluid laminar flow through helical coils. *Journal of Dispersion Science and Technology*, 34(12), pp. 1704-1712.
- [7] Dominic, A., Sarangan, J., Suresh, S. and Devah Dhanush, V.S., 2015. An experimental investigation of wavy and straight minichannel heat sinks using water and nanofluids. *Journal of Thermal Science and Engineering Application*, 7(3), pp. 310-312.
- [8] Zeinali Heris, S., Oghazian, F., Khademi, M. and saeedi, E., 2015. Simulation of convective heat transfer and pressure drop in laminar flow of Al₂O₃/water and CuO/water nanofluids through square and triangular cross-sectional ducts. *Journal of Renewable Energy and Environment*, 2, pp. 6-18.

- [9] Bahiraei, M. and Heshmatian, S., 2017. Application of a novel biological nanofluid in a liquid block heat sink for cooling of an electronic processor: Thermal performance and irreversibility considerations. *Energy Conversion Management*, 149(1), pp. 155–167.
- [10] Pourfattah, F., Abbasian Arani, A.A., Babaie, M.R., Nguyen, H.M. and Asadi, A., 2019. On the thermal characteristics of a manifold microchannel heat sink subjected to nanofluid using two-phase flow simulation. *International Journal of Heat and Mass Transfer*, 143, 118518.
- [11] Arshad, W. and Ali, H.M., 2017. Experimental investigation of heat transfer and pressure drop in a straight minichannel heat sink using TiO₂ nanofluid. *International Journal of Heat and Mass Transfer*, 110, pp. 248–256.
- [12] Ambreen, T. and Kim, M.H., 2018. Effect of fin shape on the thermal performance of nanofluid cooled micro pin-fin heat sinks. *International Journal of Heat and Mass Transfer*, 126 (Part B), pp. 245–256.
- [13] Peyghambarzadeh, S.M., Hashemabadi, S.H., Chabi, A.R. and Salimi, M., 2014. Performance of water based CuO and Al₂O₃ nanofluids in a Cu–Be alloy heat sink with rectangular microchannels. *Energy Conversion and Management*, 86, pp. 28–38.
- [14] Al-Rashed, A.A.A.A., Shahsavari, A., Rasooli, O., Moghimi, M.A., Karimipour, A. and Tran, M.D., 2019. Numerical assessment into the hydrothermal and entropy generation characteristics of biological water-silver nanofluid in a wavy walled microchannel heat sink. *International Communications in Heat and Mass Transfer*, 104, pp. 118–126.
- [15] Bahiraei, M. and Heshmatian, S., 2018. Thermal performance and second law characteristics of two new microchannel heat sinks operated with hybrid nanofluid containing graphene–silver nanoparticles. *Energy Conversion and Management*, 168, pp. 357–370.
- [16] Alfaryjat, A.A., Mohammed, H.A., Adam, N.M., Stanciu, D. and Dobrovicescu, A., 2018. Numerical investigation of heat transfer enhancement using various nanofluids in hexagonal microchannel heat sink. *Thermal Science and Engineering Progress*, 5, pp. 252–262.
- [17] Alfaryjat, A.A., Dobrovicescu, A. and Stanciu, D., 2019. Influence of heat flux and Reynolds number on the entropy generation for different types of nanofluids in a hexagon microchannel heat sink. *Chinese Journal of Chemical Engineering*, 27(3), pp. 501–513.
- [18] Narrein, K., Sivasankaran, S. and Ganesan, P., 2015. Two-phase analysis of a helical microchannel heat sink using nanofluids. *Numerical Heat Transfer, Part A: Applications*, 68(11), pp. 1266–1279.
- [19] Al-Rashed, A.A.A.A., Shahsavari, A., Rasooli, O., Moghimi, M.A., Karimipour, A. and Tran, M. D., 2019. Numerical assessment into the hydrothermal and entropy generation characteristics of biological water-silver nanofluid in a wavy walled microchannel heat sink. *International Communications in Heat and Mass Transfer*, 104, pp. 118–126.
- [20] Elias, M.M., Miqdad, M., Mahbubul, I.M., Saidur, R., Kamalisarvestani, M., Sohel, M.R., Hepbasli, A., Rahim, N.A. and Amalina, M.A., 2013. Effect of nanoparticle shape on the heat transfer and thermodynamic performance of a shell and tube heat exchanger. *International Communications in Heat and Mass Transfer*, 44, pp. 93–99.
- [21] Vanaki, Sh.M., Mohammed, H.A., Abdollahi, A. and Wahid, M.A., 2014. Effect of nanoparticle shapes on the heat transfer enhancement in a wavy channel with different phase shifts. *Journal of Molecular Liquids*, 196, pp. 32–42.
- [22] Abbasian Arani, A.A., Sadripour, S. and Kermani, S., 2017. Nanoparticle shape effects on thermal-hydraulic performance of boehmite alumina nanofluids in a sinusoidal wavy minichannel with phase shift and variable wavelength. *International Journal of Mechanical Sciences*, 128–129, pp. 550–563.
- [23] Liu, F., Cai, Y., Wang, L. and Zhao, J., 2018. Effects of nanoparticle shapes on laminar forced convective heat transfer in curved ducts using two-phase model. *International Journal of Heat and Mass Transfer*, 116, pp. 292–305.
- [24] Shahsavari, A., Rahimi, Z. and Salehipour, H., 2019. Nanoparticle shape effects on thermal-hydraulic performance of boehmite alumina nanofluid in a horizontal double-pipe minichannel heat exchanger. *Heat and Mass Transfer*, 55(6), pp. 1741–1751.
- [25] Monfared, M., Shahsavari, A. and Bahrebar, M.R., 2019. Second law analysis of turbulent convection flow of boehmite alumina nanofluid inside a double-pipe heat exchanger considering various shapes for nanoparticle. *Heat and Mass Transfer*, 135(2), pp. 1521–1532.
- [26] Bahiraei, M., Monavari, A., Naseri, M. and Moayedi, H., 2020. Irreversibility characteristics of a modified microchannel heat sink operated with nanofluid considering different shapes of nanoparticles. *International Journal of Heat and Mass Transfer*, 151, 119359.
- [27] Zahmatkesh, I., Sheremet, M., Yang, L., Zeinali Heris, S., Sharifpur, M., Meyer, J.P., Ghalambaz, M., Wongwises, S., Jing, D. and Mahian, O., 2021. Effect of nanoparticle shape on the performance of thermal systems utilizing

- nanofluids: A critical review. *Journal of Molecular Liquids*, 321, 114430.
- [28] Fan, Y., Lee, P.S., Jin, L.W. and Chua, B.W., 2013. A simulation and experimental study of fluid flow and heat transfer on cylindrical oblique finned heat sink. *International Journal of Heat and Mass Transfer*, 61, pp. 62–72.
- [29] Fan, Y., Lee, P.S., Jin, L.W. and Chua, B.W., 2014. Experimental investigation on heat transfer and pressure drop of a novel cylindrical oblique fin heat sink. *International Journal of Thermal Sciences*, 76, pp. 1–10.
- [30] Azizi, Z., Alamdari, A. and Malayeri, M.R., 2015. Convective heat transfer of Cu–water nanofluid in a cylindrical microchannel heat sink. *Energy Conversion and Management*, 101, pp. 515–524.
- [31] Azizi, Z., Alamdari, A. and Malayeri, M.R., 2016. Thermal performance and friction factor of a cylindrical microchannel heat sink cooled by Cu-water nanofluid. *Applied Thermal Engineering*, 99, pp. 970–978.
- [32] Falahat, A.R., Bahoosh, R., Noghrehabadi, A.R. and Rashidi, M.M., 2019. Experimental study of heat transfer enhancement in a novel cylindrical heat sink with helical minichannels. *Applied Thermal Engineering*, 154, pp. 585–592.
- [33] Khalifa, M.A. and Jaffal, H.M., 2019. Effects of channel configuration on hydrothermal performance of the cylindrical mini-channel heat sinks. *Applied Thermal Engineering*, 148, pp. 1107–1130.
- [34] Abdulhaleem, A.A., Jaffal, H.M. and Khudhur, D.S., 2019. Performance optimization of a cylindrical mini-channel heat sink using hybrid straight–wavy channel. *International Journal of Thermal Sciences*, 146(4), 106111.
- [35] Bahoosh, R. and Falahat, A.R., 2021. Heat transfer of nanofluid through helical minichannels with secondary branches. *Heat and Mass Transfer*, 57(1), pp. 703–714.
- [36] Xu, B., Ooi, K.T., Mavriplis, C. and Zaghoul, M.E., 2002. Evaluation of viscous dissipation in liquid flow in microchannels. *Journal of Micromechanics and Microengineering*, 13(1), pp. 53–57.
- [37] Xie, G., Chen, Zh., Sunden, B. and Zhang, W., 2013. Numerical Predictions of the Flow and Thermal Performance of Water-Cooled Single-Layer and Double-Layer Wavy Microchannel Heat Sinks. *Numerical Heat Transfer*, 63(3), pp. 201–225.
- [38] Wang, H., Chen, Zh. and Gao, J., 2016. Influence of geometric parameters on flow and heat transfer performance of micro-channel heat sinks. *Applied Thermal Engineering*, 107, pp. 870–879.
- [39] Hosseinzadeh, M., Zeinali Heris, S., Behesht, A. and Shanbedi, M., 2016. Convective heat transfer and friction factor of aqueous Fe₃O₄ nanofluid flow under laminar regime. *Journal of Thermal Analysis and Calorimetry*, 124(2), pp. 827–838.
- [40] Bejan, A., 1996. Entropy Generation Minimization. *CRC Press*, New York.
- [41] Zhai, Y.L., Xia, G.D., Liu, X.F. and Li, Y.F., 2014. Heat transfer in the microchannels with fan shaped reentrant cavities and different ribs based on field synergy principle and entropy generation analysis. *International Journal of Heat and Mass Transfer*, 68, pp. 224–233.
- [42] Bejan, A., 1982. Entropy Generation Through Heat and Fluid Flow. *1st edition*, Wiley, New York.
- [43] Chai, L., Xia, G., Zhou, M., Li, J. and Qi, J., 2013. Optimum thermal design of interrupted microchannel heat sink with rectangular ribs in the transverse microchambers. *Applied Thermal Engineering*, 51(1-2), pp. 880–889.
- [44] Mahian, O., Kianifar, A., Zeinali Heris, S. and Wongwises, S., 2014. First and second laws analysis of a minichannel-based solar collector using boehmite alumina nanofluids: Effects of nanoparticle shape and tube materials. *International Journal of Heat and Mass Transfer*, 78, pp. 1166–1176.
- [45] Zeinali Heris, S., Nasr Esfahany, M. and Etemad, S.Gh., 2007. Experimental investigation of convective heat transfer of Al₂O₃/water nanofluid in circular tube. *International Journal of Heat and Fluid Flow*, 28(2), pp. 203–210.
- [46] Corcione, M., 2011. Empirical correlating equations for predicting the effective thermal conductivity and dynamic viscosity of nanofluids. *Energy Conversion and Management*, 52(1), pp. 789–793.
- [47] Timofeeva, E.V., Routbort, J.L. and Singh, D., 2009. Particle shape effects on thermophysical properties of alumina nanofluids. *Journal of Applied Physics*, 106(1), 014304–10.